# Drag Reduction of Non-Circular Cylinder at Subcritical Reynolds Numbers

V. Suresh[1†], P. S. Premkumar[2] and C. Senthilkumar[1]

*[1]Department of Aerospace Engineering, M.I.T Campus, Anna University, Chennai, 600044, India*
*[2]Department of Aeronautical Engineering, Kumaraguru College of Technology, Coimbatore, 641049, India*

†*Corresponding Author Email:sureshvc1983@gmail.com*

## ABSTRACT

Experimental and numerical investigation of fore body geometrical effects on drag and flow-field of non-circular cylinder ( D-shaped bluff body) were conducted in the subcritical flow regime at Reynolds number in the range of 1 x $10^5 \leq$ Re $\leq 1.8$ x $10^5$. To shield the non circular cylinder ( D-shaped model ) front surface from the positive pressure of the unsteady vortex generation in the near wake, circular disk of various geometries were attached upstream of the non-circular cylinder base model. The fore body makes the streamlines that separate from its edges to attach smoothly onto the front face shoulders of the main body, thereby converting the bluff body into an equivalent streamlined body to result in low drag. The diameter of the fore body ($b_1$) ranges from 0.25 to 0.75 times the hydraulic diameter of base model ( $b_2$ ) and the gap ratio ( g/ $b_2$ ),was in the range from 0.25 to 1.75 $b_2$. The experimental and numerical investigations show that by using a circular disk as fore body with a width ratio $b_1/b_2$ of 0.75 and a gap ratio of g/ $b_2$ = 0.75 results in a configuration having percentage drag reduction of about 67 % and 65 % respectively.

Keywords: D-shaped model; Pressure drag; Shielding effect; CFD; Fore body geometry; Drag reduction.

## NOMENCLATURE

| | | | |
|---|---|---|---|
| $b_1$ | diameter of base model | g | gap |
| $b_2$ | cylinder diameter-front body | H | height |
| $C_{D_o}$ | drag coefficient for base model | O | output matrix |
| $C_D$ | drag coefficient for D-shaped model and disk | $Re_{b_2}$ | Reynolds number |
| $\Delta C_D$ | difference between above two drag coefficients | S | reference area |
| | | $V_\infty$ | free stream velocity |
| $C^{-1}$ | inverse of coefficient matrix | W | width |
| D | drag force | $\rho_\infty$ | free stream density |
| F | force matrix | | |

## 1. INTRODUCTION

The drag reduction of bluff bodies is an extensive area of research with wide range of applications, which concerns not only increasing driving speeds of automobiles, comfort, safety as well as against dwindling fuel resources and pollutants emissions. Aerodynamic configurations like buildings, cars, trucks, chimneys, wind turbine towers are all in the bluff body shape and hence to study the phenomena as well as techniques to overcome the loads acting due to the aerodynamic nature becomes vital.

For bluff bodies at subcritical Reynolds number the flow is characterized with a large wake region. These wake regions could be caused by the separated shear layers which may be influenced by the effects such as sharp corners, adverse pressure gradient, shape modifications, angle of orientation etc. The flow regimes caused by above phenomena feed vortices to wake continuously and shed downstream till the strength prevails. The aerodynamic objectives are identified and design concepts are made in the recent years of research, also necessary technology developments to fulfill these design concepts are envisaged for the recent ground transport vehicles.

Various methods have been developed to reduce the drag force on a circular cylinder in the subcritical flow regime by Choi, B. and Choi, H. ( 2000), Bouak and Lemay ( 1998 ), Isaev, *et al* ( 2002 ), Yajima and Samo ( 1996 ), Igarashi, *et al* ( 1994 ), Nabil A.H.El-Khairy

(2003 ), Panfeng Zhang *et al* ( 2006 ), Matteo Orazi *et al* ( 2014 ) and Wang J. J., *et al* ( 2006 ). For non-circular cylinders only limited work have been carried out by Khalid M.Sowoud *et al* ( 1992 ), Bandu N.Pamadi and Lakshmana Gowda ( 1987 ), E. Rathakrishnan (1999 ), Pujals *et al* ( 2010 ) and Keith Koenig and Anatol Roshko ( 1985 ). A popular method of reducing drag of such bodies is to round off the sharp corners of bluff bodies. However, the maximum drag achievable is limited to 50 %. Experiments were performed by Khalid M. Sowoud *et al*, ( 1992 ) on the non-circular cylinder model and reduction in drag was attained about 80 % for the square plate front body, whereas for the D-shaped front body is about 70 %. An application of this technique on road transport vehicles is described in the reference by Bandu N. Pamadi *et al*. (1990).

Bandu N. Pamadi and Lakshmana Gowda ( 1992 ) proposed a fluid flow mechanism that produced large drag reduction in which the flow separates at the strakes, undergoes transition to turbulence, and then smoothly reattaches back to the body at or very close to the corners. Separation bubble is formed between the strakes and the reattachment point, and this bubble generates suction on the forward face. The vortex shedding was greatly suppressed and drag reduction of about 81.5 % was achieved for the optimum strake configuration. Koenig and Roshko found that a disk mounted in front of a flat-faced axisymmetric cylinder produced significant drag reduction for some combinations of disk diameter and gap ratios. The flow mechanism associated with drag reduction was the smooth reattachment of the separated shear layers originating at the edges of the disk back to the cylinder at or very close to the shoulder. Thus the primary flow mechanisms leading to optimum drag reduction appear to be of the same nature in three-dimensional and axisymmetric flows.

## 2. EXPERIMENTAL ARRANGEMENT AND MEASURING INSTRUMENTS

### 2.1 Experimental Model

The bluff model selected is a D-shaped model (Non-circular cylinder) with $b_2$= 150 mm, 162 mm long and R ($b_2/2$) = 75 mm in radius at back. For the fore body, circular disk of 5 different base diameters varying from $0.25b_2$ to $0.75b_2$ were used. The thickness of the all front body model is 10 mm. The model dimension and setup configuration are sketched in Fig.1 (a) - (b). The gap between the front and rear bodies was varied from $0.25b_2$ to $1.75b_2$, in steps of $0.25b_2$. Model was fabricated using well-seasoned teak wood for smooth surface finish. In order to facilitate the internal balance to measure the force experienced by the model, weight of the model is adjusted in such a way that the center of gravity was close to the balance mass center.

The experiments were conducted in a low speed, open circuit wind tunnel with a test section size of 1.2 m x 0.9 m x 1.8 m ( W x H x L) having velocity range up to 40 m/s and the turbulence intensity of the wind tunnel is about 5.6 % . The wind velocity was monitored using Pitot static tube installed at the test section. Wind velocities used in the test section were 10.11 m/s, 13.89 m/s and 18.09 m/s which yields Reynolds number based on hydraulic diameter of non-circular cylinder as $Re_{b2}$ = 1 x $10^5$, 1.4 x $10^5$ and 1.8 x $10^5$, respectively.
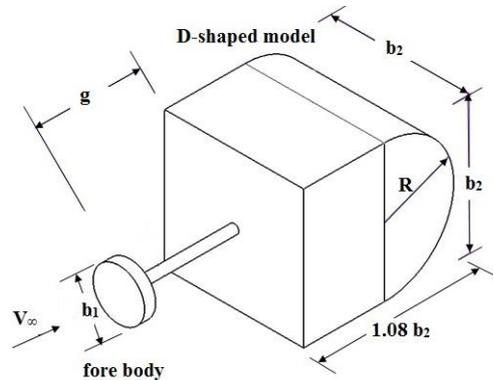


**Fig. 1a. Model nomenclature.**

The Reynolds numbers were chosen to represent the subcritical flow regime. The uncertainty of velocity is about 1.5 %.
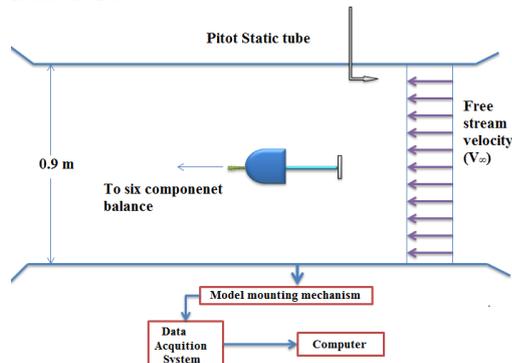


**Fig. 1b. Sketch of Experimental setup.**

Almost all the tests were performed at least twice to ensure their repeatability. It was found that the time average force were repeatable to within ± 1 %. Force measurement was performed by using six component internal strain gauge balance. The sampling frequency is 600 Hz and the total period of sampling is 10 seconds. No blockage correction was done, since all tests were made at zero angle of attack. At all runs, the blockage was only 2.34 %.

Prior to experiment, the balance was calibrated to generate inverse coefficient matrix to covert output voltage into force. Inverse co-efficient matrix is multiplied with output matrix to get the force matrix during wind-tunnel testing.

The drag force and drag coefficient were calculated from the following expressions, :

$$F = [C]^{-1}[O] \tag{1}$$

$$C_{D_o} = \frac{2D_O}{\rho_\infty V_\infty^2 S} \tag{2}$$

$$C_D = \frac{2D}{\rho_\infty V_\infty^2 S} \tag{3}$$

**Table 1 Domain independency study**

| Iteration Number | Upstream | Downstream | Farfield | Drag Coefficient ($C_{DO}$) for $V_\infty = 13.89$ m/s |
|---|---|---|---|---|
| Domain 1 | 3L | 7L | 3L | 0.914 |
| Domain 2 | 3L | 10L | 5L | 1.307 |
| Domain 3 | 4L | 12L | 5L | 1.313 |

**Table 2 Grid independency study**

| Mesh Type | First cell size $(10^{-3})$mm | Shape | No of Elements $(10^6)$ | Drag Coefficient($C_{DO}$) for $V_\infty = 13.89$ m/s |
|---|---|---|---|---|
| Coarse | 30 | Tetra | 2.1 | 1.072 |
| Medium | 52.5 | Tetra | 13.3 | 1.307 |
| Fine | 23.6 | Tetra | 19.6 | 1.318 |

## 2.2 CFD Simulation

The domain independency study was performed as shown in the Table.1. Based on the results obtained from each configuration the suitable domain with necessary boundary conditions as shown in Fig. 2a was opted for this study.
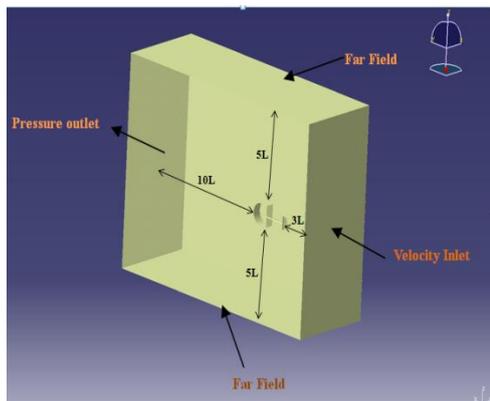


**Fig. 2a. Domain with necessary boundary conditions.**
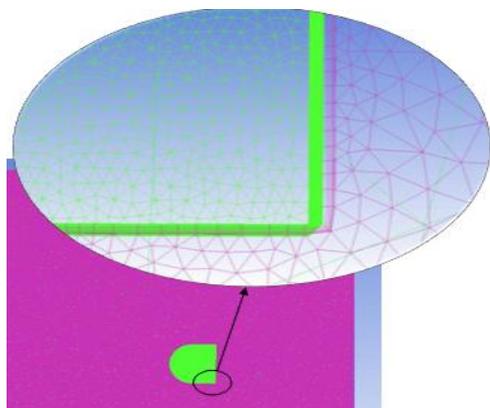


**Fig. 2b. Numerical grid around the D-shaped model.**

All the dimensions of the domain are made relative to the length of the model (L). The finite volume solver ANSYS CFX, was used to obtain the numerical solution of the Reynolds averaged Navier–Stokes (RANS) equations with k–ω (SST) turbulence model. No slip boundary condition was applied to all the surfaces of the computation domain.

and wall boundaries of the model. Uniform flow at the inlet zone of the domain was attained by applying the condition as zero boundary layer thickness and the turbulence intensity of 0.25%.

The computational cells were generated by using local refinement method and the images of numerical grid around the D-shaped model are shown in Fig. 2b The k- ω (SST) method with SIMPLE (Semi-Implicit Pressure Linked Equation) algorithm was used as an iterative scheme and considering spatial discretization gradient as least squares cell based method. The pressure, momentum, turbulent kinetic energy and turbulent dissipation rate were set to follow the second order upwind scheme for iterating the numerical simulation.

The inlet velocity of air was given as 13.89 m/s relative to the experimental Reynolds number of the model. The grid independence test was carried out prior to the CFD simulation because the number of cells in the fluid domain has considerable impact in affecting the results of CFD analysis. The results of grid independency test are illustrated in Table. 2. The entire fluid domain was discretized with 5 prism layered mesh composed of 13 million elements by considering the initial grid layer height of 0.9 µm as the standard level of grid for all the cases.

The computationally predicted drag is slightly lower than the experimental results. However, the coefficient of drag for the model obtained from the results of wind tunnel and computational methods were closely correlating with each other by showing maximum deviation of about 8.4 %. Hence, it is evident that the numerical model predicted the drag coefficients closer to the results of experimental analysis.

**Table 3 Drag coefficient of D-shaped model ( base model )**

| Reynolds Number | Drag Coefficient ( $C_{DO}$ ) | | |
|---|---|---|---|
| | Experiment | CFD | Khalid *et al* |
| $1.0 \times 10^5$ | 1.19 | 1.29 | 1.28 |
| $1.4 \times 10^5$ | 1.32 | 1.30 | 1.39 |
| $1.8 \times 10^5$ | 1.38 | 1.31 | 1.42 |

## 3.    RESULTS AND DISCUSSION

### 3.1 Drag Coefficient of Non-Circular Cylinder (D-Shaped Model) Alone

The first configuration studied was D-shaped model with $b_2$= 150 mm and $R_2$ = 75 mm, where $R_2$ is radius of rounded back curvature. The values of drag coefficient $C_{DO}$ of the rear body was obtained from computational results was compared with experimental data and Khalid M. Sowoud *et al* (1992) as shown in Table 3.

The total drag consists of skin friction, pressure drag due to flow separation and base drag. In the model, sting is attached to base. This may also influence the base drag of the model. However in this paper, the relative effect of the total drag is considered by placing the fore body, so that influence of the sting is neglected. The difference between the drag coefficient in the present study and the Khalid M. Sowoud *et al* (1992) could be due to model support system. The high drag coefficient for the rear body $C_{DO}$ in the range of 1.19 to 1.38 is due to suction pressure at the downstream and high positive pressure experienced at the front face shown in Fig. 3.
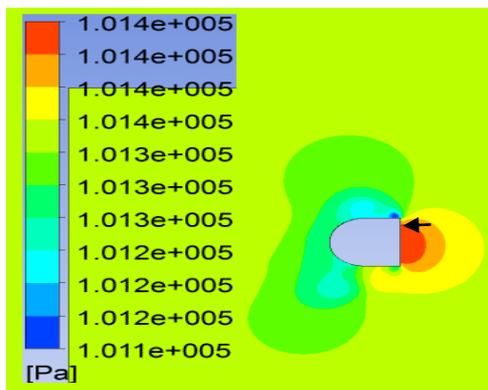


**Fig. 3. Pressure distribution around D-shaped model at a velocity of 13.89 m/s.**

This integrated effect is felt in the form of a large drag force on the rear body. The velocity contours are shown in Fig. 4. A direct study of the vortex shedding phenomenon was not attempted in this work and the presented results are steady state values though the flow is oscillatory.

### 3.2    Drag Coefficient of D-Shaped Model with Circular Disk Fore Body

This combination involved a rear body an a circular disk fore body with flat portion of front body facing flow direction. Combined drag coefficient $C_D$ for

different diameter ratios ($b_1/b_2$= 0.25, 0.37, 0.50, 0.625 and 0.75) are measured as the gap ratio $g/b_2$ changes from $0.25b_2$ to $1.75b_2$, monotonically with increments of $0.25b_2$.

Each combination of the front and rear body models was tested for three free-stream speeds, and the corresponding Reynolds numbers based on hydraulic diameter ($b_2$) of rear body are $1 \times 10^5$, $1.4 \times 10^5$ and $1.8 \times 10^5$, respectively. The results are plotted for each front body geometry and are discussed separately for each front body.
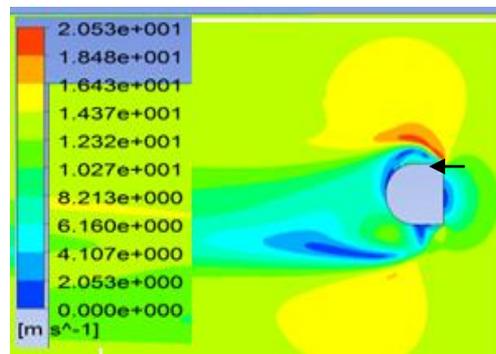


**Fig. 4. Velocity contours of D-shaped model at a velocity of 13.89 m/s.**

**Table 4 Comparison of drag coefficients obtained by CFD and experiment for D-shaped model with a disk of $b_1/b_2 = 0.25$ at a velocity of 13.89 m/s**

| $\dfrac{g}{b_2}$ | $C_D$ | | $\dfrac{C_D}{C_{D_o}}$ | |
|---|---|---|---|---|
| | CFD | EXP | CFD | EXP |
| 0.25 | 1.18 | 1.23 | 0.91 | 0.92 |
| 0.50 | 0.858 | 0.78 | 0.66 | 0.58 |
| 0.75 | 0.653 | 0.68 | 0.502 | 0.51 |
| 1.00 | 0.615 | 0.63 | 0.473 | 0.48 |
| 1.25 | 0.666 | 0.68 | 0.51 | 0.51 |
| 1.50 | 0.785 | 0.73 | 0.61 | 0.55 |
| 1.75 | 0.889 | 0.86 | 0.68 | 0.65 |

### 3.2.1    CFD Simulation for D-Shaped Model With a Disk of $b_1/b_2$= 0.25

For D-shaped model with a disk of $b_1/b_2$=0.25, all possible combinations for disk and base model are simulated for a velocity of 13.89 m/s and the drag coefficient results obtained by CFD and experiment

were compared in the Table 4.
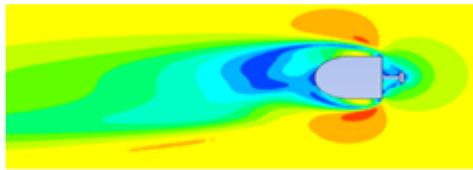


(a) D-shaped model with a disk at gap g/b₂ = 0.25
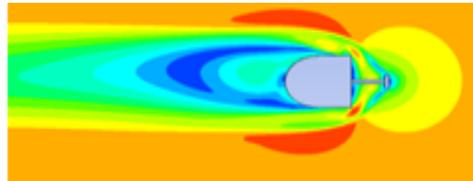


(b) D-shaped model with a disk at gap g/b₂ = 0.5
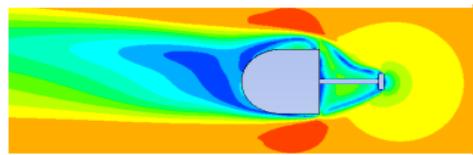


(c) D-shaped model with a disk at gap g/b₂ = 0.75
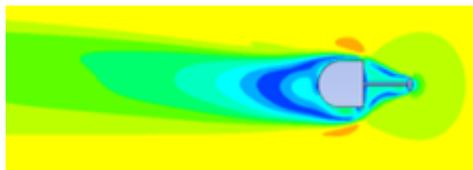


(d) D-shaped model with a disk at gap g/b₂ = 1.0 (optimum case)
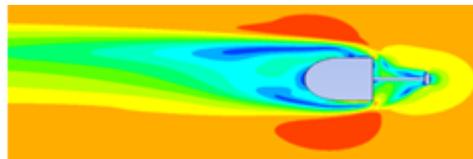


(e) D-shaped model with a disk at gap g/b₂ = 1.25
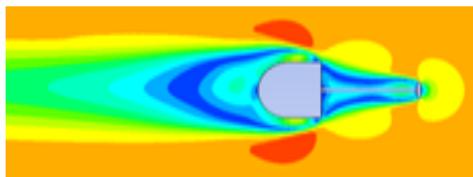


(f) D-shaped model with a disk at gap g/b₂ = 1.5
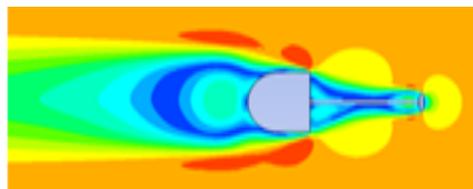


(g) D-shaped model with a disk at gap g/b₂ = 1.75

**Fig. 5. Velocity contours for D-shaped model with a disk ($b_1/b_2 = 0.25$) at a velocity of 13.89 m/s.**

When the disk is close to the D-shaped model (g/b₂=0.25 - 0.75), the separated shear layers originating at the edges of disk open out, forming a large wake and no reattachment of the flow ever occurs. Strong, alternate, instantaneous vortex shedding continues to occur as observed for the basic model as shown in Fig. 5(a-c). The drag coefficient still remains high although some reduction is obtained when compared to that of the base model.
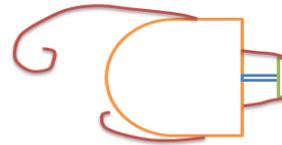


(a) gap g/b₂ =0.25
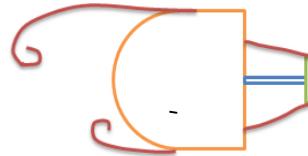


(b) gap ratio g/b₂ =0.5
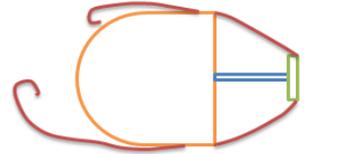


(c) gap ratio g/b₂ =0.75
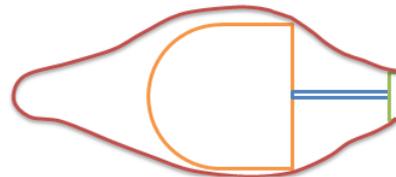


(d) gap ratio g/b₂ =1.0
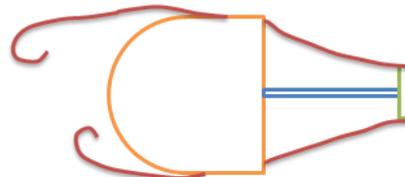


(e) gap ratio g/b₂ =1.25
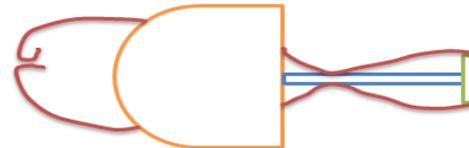


(f) gap ratio g/b₂ =1.50
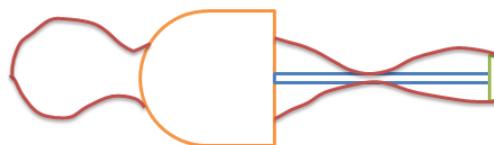


(g) gap ratio g/b₂ =1.75

**Fig. 6. Schematic of wake-profile and vortex pattern for D-shaped model with a disk ($b_1/b_2$=0.25) for a velocity of 13.89 m/s.**

At the optimum gap ($g^*/b_2 = 1$), the separated shear layers reattaches smoothly at or close to the corners of the D-shaped model as shown in Fig. 5(d). With this flow pattern , vortex shedding is very much suppressed resulting in a sharp decrease in the drag coefficient.

At larger gap ratios ($g/b_2 = 1.25 - 1.75$),the separated shear layer and reattaches on the flat face of the D-shaped model but cannot negotiate the sharp corners and separate at the corners, forming a large wake as shown in Figs. 5(e) - (g). Once again , strong , alternate, instantaneous, vortex shedding occurs in the wake. The base suction is high and the drag coefficient increases to the value of D-shaped model.

Also schematic of wake – profile were drawn out from these velocity vectors for the above cases as shown in Fig. 6 (a)-(e).

### 3.2.2 Experimental Results

From Fig. 7, the drag coefficient ratio for a small gap ratio ($g/b_2 = 0.25$) attains the maximum values of 0.98, 0.93 and 0.92 which are 2, 7 and 8 percent below the $C_{Do}$ for rear body alone, for corresponding free stream velocities. At the gap ratio of 1.0, the drag coefficient has reached the optimum case with $C_D^*/C_{Do} = 0.47$, 0.48 and 0.47 which are 53, 52 and 53 percent below the $C_{Do}$ for rear body alone, for the corresponding the Reynolds numbers.
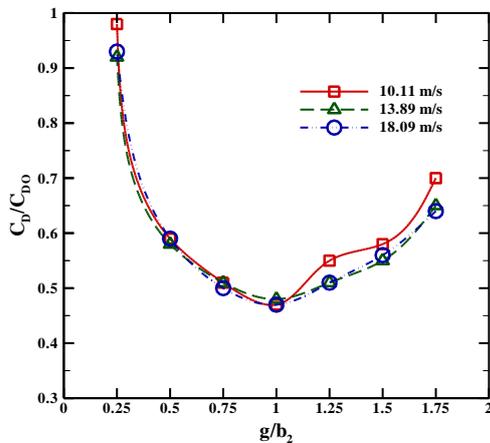


**Fig. 7. Drag coefficient for the D-shaped model with a disk of $b_1/b_2 = 0.25$.**

For $b_1/b_2 = 0.37$, Fig. 8 shows the variation of drag coefficient with the gap ratio and free stream velocity. For a gap ratio of 0.25, the drag coefficient values are 0.85, 0.80 and 0.81 which are 15, 20 and 19 percent below the $C_{Do}$ for rear body alone. When the gap ratio increased ($g^*/b_2 = 1.25$) the combined drag coefficient is decreased reaching the optimum case with $C_D^*/C_{Do} = 0.46$, 0.44 and 0.44 which are 54, 56 and 56 percent below the $C_{Do}$ for rear body alone, for the corresponding free stream velocities.

For $b_1/b_2 = 0.5$, Fig. 9 shows the variation or drag coefficient with the gap ratio and free stream velocity. For a gap ratio of 1.25 the drag coefficient values are 0.46, 0.45 and 0.46 which are 54, 55 and

54 percent below the $C_{Do}$ for rear body alone, When the gap ratio is increased or decreased from this optimum value the $C_D$ increases.
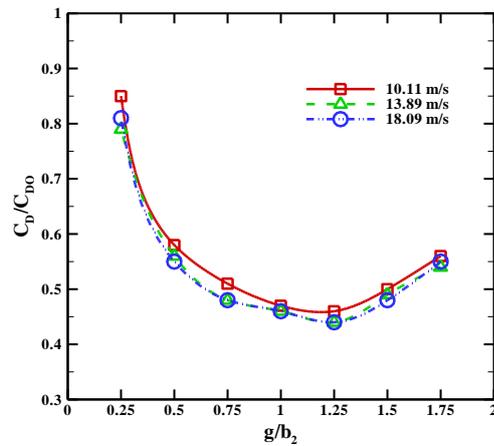


**Fig. 8. Drag coefficient for the D-shaped model with a disk of $b_1/b_2 = 0.37$.**
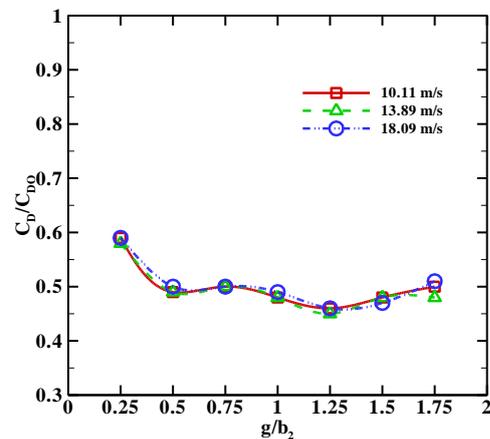


**Fig. 9. Drag coefficient for the D-shaped model with a disk of $b_1/b_2 = 0.5$.**

For $b_1/b_2 = 0.625$, Fig. 10 shows the variation of drag coefficient $C_D$ with the gap ratio and free stream velocity. All the three curves are similar in behavior, reaching the minimum at a gap ratio of 0.50 with values $C_D^*/C_{Do} = 0.43$, 0.41 and 0.40 which are 57, 59 and 60 percent below the $C_{Do}$ for rear body alone, respectively. Hence, the separated boundary layers reattach onto or very close to the rear body corners. Maximum drag reduction for the optimum case (i.e. $b_1^*/b_2 = 0.625$ and $g^*/b_2 = 0.50$) is slightly greater than the former optimum case (i.e. $b_1^*/b_2 = 0.5$ and $g^*/b_2 = 1.25$).

Beyond the optimum case, for the gap ratio in the range of 0.75 to 1.75, the drag coefficient increases or percentage drag reduction decreases with increasing gap ratio, reaching the maximum value at gap ratio 1.75 with value 0.55, 0.53 and 0.53 which are 45, 47 and 47 percent below the $C_{Do}$ for rear body alone, respectively.

For $b_1/b_2 = 0.75$, Fig. 11 shows the drag coefficient variation with the gap ratio $g/b_2$ and free stream

velocity. All the three curves are similar in behavior. For velocity 10.11 m/s, the drag coefficient curve reaches the optimum value with $C_D^*/ C_{D_o} = 0.33$ at gap ratio $g^*/b_2 = 0.75$, which is 67 % percent below the $C_{D_o}$ for rear body alone.
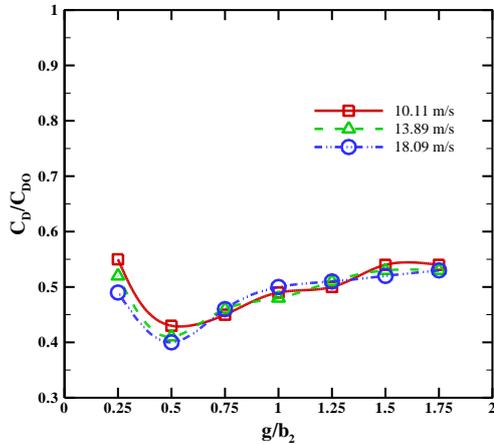


**Fig. 10. Drag coefficient for the D-shaped model with a disk of $b_1/b_2 = 0.625$.**
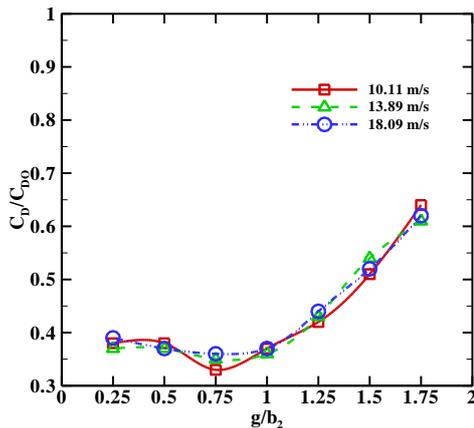


**Fig. 11. Drag coefficient for the D-shaped model with a disk of $b_1/b_2 = 0.75$.**

The optimum combinations for other cases indicate that the separated boundary layers from the edges of front body, reattached at or near the corners of rear body. The corresponding velocity stream line is shown in Fig. 12 (a) - (d).

For a gap ratio between 1.0 to 1.75, all the drag coefficients obtained are more than the optimum $C_D^*$ for rear body alone. This is because, the separated boundary layers from the edges of front body, reattached on the face of the rear body and again separated from its corners. In this case there are two wake zones, first one, behind the front body and second behind the rear body.

For velocity 13.89 m/s and 18.09 m/s, the two drag coefficient curves are similar in behavior, both reached a minimum drag coefficient at $g^*/ b_2 = 0.75$ with value $C_D^*$ $C_D^*/ C_{D_o} = 0.35$ and 0.36, which are 65 and 64 percent below the $C_D$ for rear body alone, respectively.

According to the present results, the minimum drag coefficient for circular disk front body at Re = 1.0 x

$10^5$, can be achieved only when $b_1/b_2 = 0.75$ and gap ratio $g^*/ b_2 = 0.75$, as shown in Table 5.
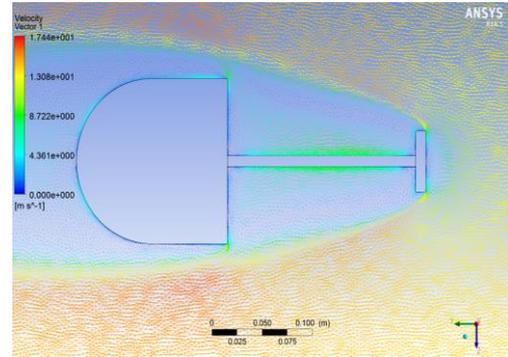


**Fig. 12(a). Streamlines for $b_1/b_2 = 0.37$ atg*/b$_2$=1.25 for a velocity of 13.89 m/s.**
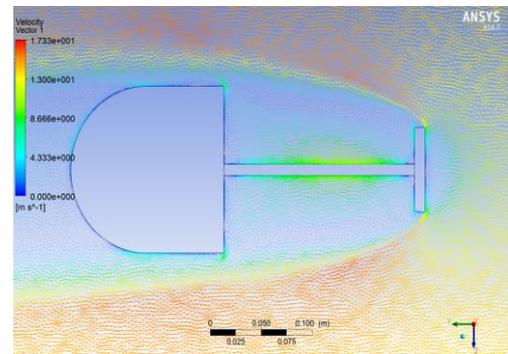


**Fig. 12(b). Streamlines for $b_1/b_2$=0.5 at g*/ b$_2$=1.25 for a velocity of 13.89m/s.**
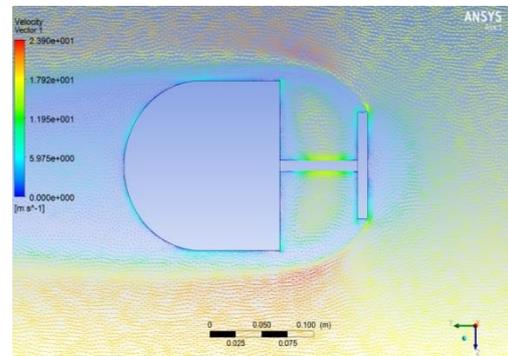


**Fig. 12(c). Streamlines for $b_1/b_2$=0.625 at g*/ b$_2$= 0.5) for a velocity of 18.09 m/s.**
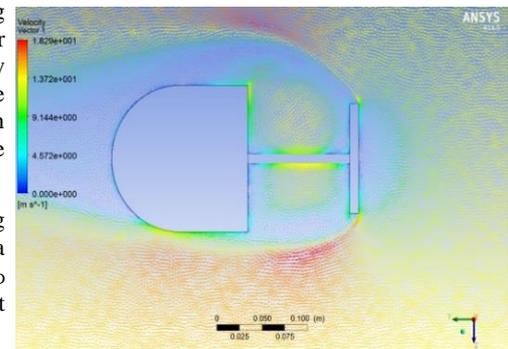


**Fig. 12(d). Streamlines for $b_1/b_2$=0.75 at g*/b$_2$=0.75 for a velocity of 13.89 m/s.**

**Table 5 Lowest drag coefficient and corresponding percentage of drag reduction for D-shaped model with a circular disk**

| $\dfrac{b_1}{b_2}$ | $\dfrac{g}{b_2}$ | $\dfrac{C_D}{C_{D_o}}$ | | | $\dfrac{\Delta C_D}{C_{D_o}}$ x 100% | | |
|---|---|---|---|---|---|---|---|
| | | $V_1$ | $V_2$ | $V_3$ | $V_1$ | $V_2$ | $V_3$ |
| 0.25 | 1.00 | 0.47 | 0.48 | 0.47 | 53 | 52 | 53 |
| 0.37 | 1.25 | 0.46 | 0.44 | 0.44 | 54 | 56 | 56 |
| 0.50 | 1.25 | 0.46 | 0.45 | 0.46 | 54 | 55 | 54 |
| 0.625 | 0.50 | 0.43 | 0.41 | 0.40 | 57 | 59 | 60 |
| 0.75 | 0.75 | 0.33 | 0.35 | 0.36 | 67 | 65 | 64 |

where $V_1$ = 10.11 m/s, $V_2$ = 13.89 m/s & $V_3$ = 18.09 m/s

## 4. CONCLUSION

From the above discussions it can be summarized that, the combination of the bluff bodies in tandem with the appropriate choice of diameter and gap ratios results always lesser drag than the drag of rear body alone ($C_{D_o}$). Streamlining effect of the fore body for the tested $b_1/b_2$ ratios is favourable upto a gap ratio of 1.25 for all geometries of circular disk. As $b_1/b_2$ increases, the gap ratio for which minimum drag occurs, reduces. Further it can be concluded that, non-circular cylinder (D-shaped) model with disk front body 0.75 times diameter of the disk and the corresponding gap is 0.75 times the hydraulic diameter of base resulted in the maximum drag reduction of 67 percent.

## REFERENCES

Choi, B. and H. Choi (2000). Drag Reduction with a Sliding Wall in a Flow over a Circular Cylinder. *AIAA Journal.* 38(4), 715-717.

Hoerner, S. F (1965). *Fluid Dynamic Drag.* Brick Town, New Jersey.

Khalid M. Sowoud and E. Rathakrishnan (1992). Front Body Effects on Drag and Flow field of a Three-Dimensional Noncircular Cylinder. *AIAA Journal.* 37(7), 1345-1347.

Koenig, K. and A. Roshko (1985). An experimental study of geometrical effects on the drag and flow field of two bluff bodies separated by a gap. *Journal of Fluid Mechanics.* 156(July), 167-204.

Nabil, A. H. El-Khairy (2003). Drag reduction of a circular cylinder at subcritical flow regime using base shield plates. *Wind and Structures.* 6(5), 347-356.

Orazi, M., D. Lasagna and G. Iuso (2014).Circular Cylinder Drag Reduction Using Piezoelectric Actuators. *Advances in Aircraft and spacecraft Science.* 1(1), 27-41.

Pamadi, B. N. and B. H. Laxmana Gowda (1992). Cross flow Aerodynamic Characteristics of a Noncircular Cylinder With and Without Strakes. *AIAA Journal.* 30(12), 2864-2870.

Pamadi, B. N., C. Pereira and B. H. Laxman Gowda (1988). Drag Reduction by Strakes of Noncircular Cylinders. *AIAA Journal* 26(3), 292 - 299.

Pamadi, B. N., L. W. Taylor and T. O. Leary (1990, January). A method Aerodynamic Drag of Road Vehicle. *NASA Technical Memorandum.* Langley Research Center, Hampton, United States.

Pujals, G., S. Depardon and C. Cossu (2010). Drag reduction of a 3D bluff body using coherent streamwise streaks. *Experiments in Fluids.* 49, 1085-1094.

Rathakrishnan, E. (1999). Effect of Splitter Plate on Bluff Body Drag. *AIAA Journal.* 37(9). 1125 - 1126.

Zhang, P., L. Gao and J. Wang (2006). Drag Reduction of a disk with an upstream rod. *Wind and Structures.* 9(3), 245-254.